Time-Reversed Lasing and Interferometric Control of Absorption

Wenjie Wan, *et al.*

Science **331**, 889 (2011);
DOI: 10.1126/science.1200735

6. V. Garcia *et al.*, *Nature* **460**, 81 (2009).
7. H. Kroemer, *Surf. Sci.* **132**, 543 (1983).
8. J. Mannhart, D. G. Schlom, *Science* **327**, 1607 (2010).
9. A. Ohtomo, H. Y. Hwang, *Nature* **427**, 423 (2004).
10. N. Nakagawa, H. Y. Hwang, D. A. Muller, *Nat. Mater.* **5**, 204 (2006).
11. Y. Hotta, T. Susaki, H. Y. Hwang, *Phys. Rev. Lett.* **99**, 236805 (2007).
12. A. Brinkman *et al.*, *Nat. Mater.* **6**, 493 (2007).
13. N. Reyren *et al.*, *Science* **317**, 1196 (2007).
14. Y. Kozuka *et al.*, *Nature* **462**, 487 (2009).
15. S. Thiel, G. Hammerl, A. Schmehl, C. W. Schneider, J. Mannhart, *Science* **313**, 1942 (2006).
16. C. Cen *et al.*, *Nat. Mater.* **7**, 298 (2008).
17. C. Cen, S. Thiel, J. Mannhart, J. Levy, *Science* **323**, 1026 (2009).
18. S. Okamoto, A. J. Millis, *Nature* **428**, 630 (2004).
19. Y. Okimoto, T. Katsufuji, Y. Okada, T. Arima, Y. Tokura, *Phys. Rev. B* **51**, 9581 (1995).
20. Materials and methods are available as supporting material on *Science* Online.
21. H. D. Zhou, J. B. Goodenough, *J. Phys. Condens. Matter* **17**, 7395 (2005).
22. K. Janicka, J. P. Velev, E. Y. Tsymbal, *Phys. Rev. Lett.* **102**, 106803 (2009).
23. M. Imada, A. Fujimori, Y. Tokura, *Rev. Mod. Phys.* **70**, 1039 (1998).
24. F. J. Wong *et al.*, *Phys. Rev. B* **81**, 161101 (2010).
25. H. Ishida, A. Liebsch, *Phys. Rev. B* **77**, 115350 (2008).
26. S. Okatov, A. Poteryaev, A. Lichtenstein, *Europhys. Lett.* **70**, 499 (2005).
27. Z. S. Popovic, S. Satpathy, *Phys. Rev. Lett.* **94**, 176805 (2005).
28. S. Okamoto, A. J. Millis, N. A. Spaldin, *Phys. Rev. Lett.* **97**, 056802 (2006).
29. R. Pentcheva, W. E. Pickett, *Phys. Rev. Lett.* **99**, 016802 (2007).
30. M. Breitschaft *et al.*, *Phys. Rev. B* **81**, 153414 (2010).
31. G. Kotliar *et al.*, *Rev. Mod. Phys.* **78**, 865 (2006).
32. Q. Si, M. J. Rozenberg, G. Kotliar, A. E. Ruckenstein, *Phys. Rev. Lett.* **72**, 2761 (1994).

33. We thank D. G. Schlom and D. A. Muller for fruitful discussions. This work was supported by the National Science Foundation under grant DMR-0906443 and a David and Lucile Packard Fellowship (C.B.E.). The research at University of Nebraska was supported by the Materials Research Science and Engineering Center (NSF grant DMR-0820521), the Nanoelectronics Research Initiative of the Semiconductor Research Corporation, the National Science Foundation (grant EPS-1010674), and the Nebraska Research Initiative. Work at the University of Michigan was supported by the U.S. Department of Energy (DOE) under grant DE-FG02-07ER46416. We thank the National Center for Electron Microscopy at Lawrence Berkeley National Laboratory for their support under DOE grant DE-AC02-05CH11231 for user facilities. Work at Argonne and use of the Advanced Photon Source were supported by the DOE Office of Science, Office of Basic Energy Sciences, under contract DE-AC02-06CH11357. Work at Brookhaven National Laboratory was sponsored by DOE/BES/MSE and the Center for Functional Nanomaterials under contract DE-AC02-98CH10886. J. Karapetrova's assistance at beamline 33-BM of the Advanced Photon Source is gratefully acknowledged.

Supporting Online Material

www.sciencemag.org/cgi/content/full/331/6019/886/DC1
Materials and Methods
Figs. S1 to S8
Table S1
References

7 October 2010; accepted 19 January 2011
10.1126/science.1198781

Time-Reversed Lasing and Interferometric Control of Absorption

Wenjie Wan, Yidong Chong, Li Ge, Heeso Noh, A. Douglas Stone, Hui Cao*

In the time-reversed counterpart to laser emission, incident coherent optical fields are perfectly absorbed within a resonator that contains a loss medium instead of a gain medium. The incident fields and frequency must coincide with those of the corresponding laser with gain. We demonstrated this effect for two counterpropagating incident fields in a silicon cavity, showing that absorption can be enhanced by two orders of magnitude, the maximum predicted by theory for our experimental setup. In addition, we showed that absorption can be reduced substantially by varying the relative phase of the incident fields. The device, termed a "coherent perfect absorber," functions as an absorptive interferometer, with potential practical applications in integrated optics.

Time-reversal symmetry is a fundamental symmetry of classical electromagnetic theory and of nonrelativistic quantum mechanics. It implies that if a particular physical process is allowed, then there also exists a "time-reversed process" that is related to the original process by reversing momenta and the direction of certain fields (typically external magnetic fields and internal spins). These symmetry operations are equivalent to changing the sign of the time variable in the dynamical equations, and for steady-state situations they correspond to interchanging incoming and outgoing fields.

The power of time-reversal symmetry is that it enables exact predictions of the relationship between two processes of arbitrary complexity. A familiar example is spin echo in nuclear magnetic resonance (NMR) (*1*): A set of precessing spins in a magnetic field fall out of phase because of slightly different local field environments, quenching the NMR signal. The signal can be restored by imposing an inversion pulse at time T, which has the effect of running the phase of each spin backward in time, so that after $2T$ they are back in phase, no matter how complicated their local field environment. Time-reversal symmetry is the origin of the well-known weak localization effect (*2*) in the resistance of metals, the coherent backscattering peak in the reflection from multiple scattering media (*3*–*5*), and the elastic enhancement factor familiar in nuclear scattering (*6*). Effects due to direct generation of time-reversed waves via special "mirrors" have been extensively studied for sound waves (*7*–*9*) and microwave radiation (*10*).

Recently, several of the authors (*11*) explored theoretically an exact time-reversal symmetry property of optical systems: the time-reversed analog of laser emission. In the lasing process, a cavity with gain produces outgoing optical fields with a definite frequency and phase relationship, without being illuminated by coherent incoming fields at that frequency. The laser is coupled to an energy source (the pump) that inverts the electron population of the gain medium, causing the onset

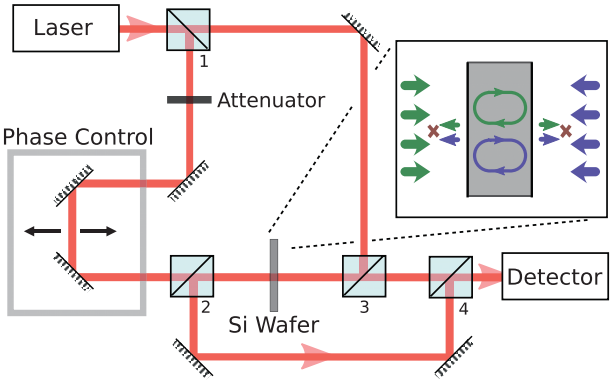

Fig. 1. A laser beam from a tunable (800 to 1000 nm) continuous-wave Ti:sapphire source enters a beam splitter (designated 1). The two split beams are directed normally onto opposite sides of a silicon wafer of thickness ~110 μm, using a Mach-Zehnder geometry. A phase delay in one of the beam paths controls the relative phase of the two beams. An additional attenuator ensures that the input beams have equal intensities, compensating for imbalances in the beam splitters and other imperfections. The output beams are rerouted, via beam splitters (designated 2, 3, and 4), into a spectrometer. The inset is a schematic of the CPA mechanism. The incident beams from left and right multiply scatter within the wafer with just the right amplitude and phase so that the total transmitted and reflected beams destructively interfere on both sides, leading to perfect absorption.

Department of Applied Physics, Post Office Box 208284, Yale University, New Haven, CT 06520, USA.

*To whom correspondence should be addressed. E-mail: hui.cao@yale.edu

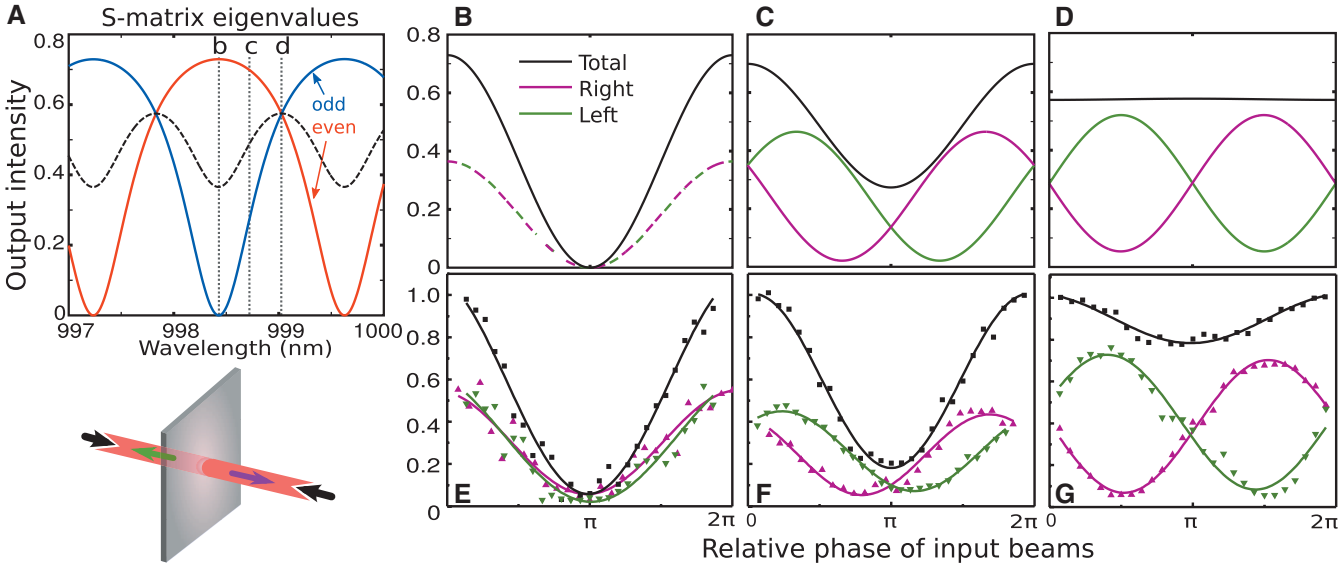

Fig. 2. Phase modulation of beam absorption. (**A**) Theoretical plot of normalized total output intensities as a function of wavelength λ for parity-odd (blue) and parity-even (red) scattering eigenmodes. The dashed black line is the result for incoherent input beams. (**B** to **D**) Theoretical output intensities at three representative values of λ as the relative phase of the input beams is varied, showing intensities emitted to the right (magenta) and left (green) sides of the slab, and the total intensity (black). Values of λ corresponding to (B) to (D) are marked by vertical lines in (A); (B) is the CPA resonance. (**E** to **G**) Experimental results at values of λ approximately corresponding to (B) to (D). Solid lines are fits to the data, not theory curves; results are normalized to max(I_{out}) of the fit.

of coherent radiation at a threshold value of the pump. Above threshold the laser is a nonlinear device, but at threshold for the first lasing mode, the laser is described by the linear Maxwell equations with complex (amplifying) refractive index. Because of the properties of these equations under time reversal (*11*), it follows that the same cavity, with the gain medium replaced by an equivalent absorbing medium, will perfectly absorb the same frequency of light, if it is illuminated with incoming waves with the same field pattern. Additional analysis showed that if the cavity is illuminated with coherent field patterns not corresponding to the time-reversed emission pattern, it is possible to decrease the absorption well below the value for incoherent illumination. Such a device, related to a laser by time reversal, was termed a "coherent perfect absorber" (CPA) (*11*). The properties of CPAs point to a new method for controlling absorption through coherent illumination. Here we demonstrate both the strong enhancement and reduction of absorption in a simple realization of the CPA: a silicon wafer functioning as solid Fabry-Perot etalon.

We now give a more precise statement of the CPA theorem. For simplicity, consider the scalar wave equation [see (*12*) for the vector generalization]:

$$[\nabla^2 + n^2(\mathbf{r})k^2]\phi_k(\mathbf{r}) = 0 \qquad (1)$$

where $k = \omega/c$, ω is the frequency, c is the speed of light, $\phi_k(\mathbf{r})$ is the electric field, and $n = n_1 + in_2$ is the refractive index ($n_2 < 0$ for gain and $n_2 > 0$ for absorption). Outside of the cavity, n is assumed to be real and constant. Steady-state solutions of these equations are described by the electromagnetic scattering matrix (S-matrix) (*11*),

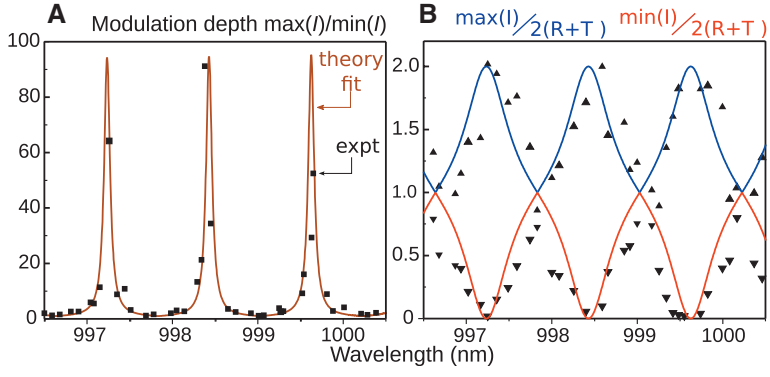

Fig. 3. (**A**) Modulation depth—the ratio of maximum to minimum output intensity obtained by varying the relative input phase, $M = \max(I_{out})/\min(I_{out})$—as a function of wavelength. The wavelength spacing of adjacent M-peaks is ~1.27 nm, closely matching the free spectral range of the Si etalon. Between these maxima, M goes nearly to unity, corresponding to the "phase-insensitive points" where the two S-matrix eigenvalues have the same magnitude. (**B**) Ratio of these maximum and minimum values to the value $2(R + T)$, obtained when the two input beams do not interfere coherently, demonstrating both enhancement and suppression of cavity absorption by interference. Squares (A) and triangles (B) are experimental data [in (B), upright triangles denote reduced absorption, whereas inverted triangles denote enhanced absorption]; solid curves are theory, including resolution effects (*12*).

which relates incoming and outgoing channel states whose weights are represented by complex vectors α, β, obeying

$$\mathbf{S}[n(\mathbf{r})k] \cdot \alpha = \beta \qquad (2)$$

The S-matrix is unitary if and only if $n_2 = 0$. In general it satisfies the property that, under time reversal,

$$\mathbf{S}[n^*(\mathbf{r})k] \cdot \beta^* = \alpha^* \qquad (3)$$

Equations 2 and 3 imply that every scattering solution of the amplifying problem, with $n = n_1 - in_2$ ($n_2 > 0$) and outgoing amplitudes β, is accompanied by a solution to the absorbing problem with $n = n_1 + in_2$ and incoming amplitudes β*.

Now consider a laser at threshold: There exists a specific solution, described by a vector of nonzero outgoing amplitudes β (determined up to an overall scale factor), for infinitesimal incoming amplitudes ($\alpha \to 0$). Thus, the S-matrix has an eigenvalue that tends to infinity. By the time-reversal property (Eq. 3), a lossy cavity with $n_1 = n_1$, $-n_2 \to +n_2$ must possess a solution corresponding to the time-reversed lasing mode, for which the incident field (β*) is completely absorbed ($\alpha^* \to 0$); the associated S-matrix

eigenvector has eigenvalue zero. This lossy cavity is the CPA, the time-reversed counterpart to the original laser. Furthermore, if the CPA cavity is accessible by more than one asymptotic channel, it typically possesses other eigenvectors with nonzero eigenvalues, so there are many other incident radiation patterns, at the same frequency, that are not fully absorbed.

Early laser studies (*13*, *14*) had briefly noted the possibility of the time-reversed process of lasing, but detailed theory and investigation of practical realizations began with (*11*). The simplest realization, a single-channel CPA, consists of an asymmetric cavity with a perfectly reflecting mirror at one end and coupled at the other end to a single input channel. When the absorption of the cavity is tuned to an optimal value, the reflection from the "back mirror" of the cavity destructively interferes with the reflection from the front face, and the incident radiation is perfectly absorbed. Several investigators have discovered the coherent absorption effect for this case, without making use of the analogy to a laser at threshold. III-V semiconductor devices that are essentially equivalent to the single-channel CPA have been widely developed over the past two decades as modulators (*15*–*18*) ("asymmetric Fabry-Perot" modulators) and detectors (*19*, *20*) ("resonant cavity-enhanced photodetectors"). In addition, a closely related device, used as an optical switch or filter, is the "critically coupled resonator" (*21*–*23*), which typically has a ring geometry and is equivalent to two decoupled single-channel CPAs.

Our two-channel CPA is qualitatively different from the single-channel case because it requires two coherent input beams, and perfect absorption is only achieved when these beams have the correct relative phase and amplitude. Thus, it is not only sensitive to frequency but to the amplitude and phase of the input light and can function as an absorptive interferometer, potentially useful as a modulator, detector, or phase-controlled optical switch.

Reaching the precise CPA condition of perfect absorption requires tuning two parameters (e.g., n_1 and n_2 or n_2 and λ); by analogy to the laser, the CPA must have the correct absorption to reach "threshold" and also must satisfy an appropriate interference condition in the cavity. However, simply tuning λ near the band gap of a semiconductor (*11*) can bring the system very close to the CPA condition, increasing the absorption by many orders of magnitude.

The simplest two-channel CPA has a uniform complex refractive index n approaching one of the values needed for the CPA condition, connected to a single propagating mode on the left and another on the right. In our implementation (Fig. 1), two collimated counterpropagating free-space laser beams are directed onto opposite surfaces of a Si wafer, which functions as a low-Q Fabry-Perot etalon based on Fresnel reflection at the surfaces ($Q \approx 840$). Although these illumination conditions are not truly single-channel because of the finite width of the free-space beams, our results indicate that this is not the main source of deviation from the ideal behavior (*12*). The output beams are collected into a high-resolution spectrometer, and the intensities in each individual output beam, as well as the total output intensity, are measured (*12*).

In this geometry, the physical origin of the CPA effect is clear (*11*). As illustrated in the inset of Fig. 1, the multiply scattered transmission from the left beam interferes destructively with the multiply scattered reflection from the right beam at the right interface, and vice versa at the left face. At the precise CPA condition, this leads to an ideal interference "trap" for the two beams, so that eventually the radiation is entirely dissipated by the interband absorption processes in the silicon. Counterintuitively, increasing the single-pass absorption would actually reduce the net absorption by disturbing the ideal balance of absorption and interference at the operating wavelength.

For a given cavity Q-value, only a certain narrow range of absorption coefficients will yield strong CPA resonances. The reflection symmetry of our cavity implies that CPA resonances arise when the reflectance (R) and transmittance (T) are equal, which occurs as λ varies through the band gap and strong absorption sets in. We use this condition to determine the operating wavelength range of 990 nm $<\sim \lambda <\sim$ 1010 nm for our system (*12*); fine-tuning λ within this interval yields strong CPA resonances.

The key quantity measured in the experiment is the total intensity of the scattered radiation (reflectance plus transmittance from both sides). This is determined theoretically by the eigenvectors of the 2 × 2 S-matrix, which satisfy $\mathbf{S}(\mathbf{k}) \cdot \alpha_i = s_i \alpha_i$ for $i = 1, 2$. Because of the cavity's reflection symmetry, the eigenvectors take the form $\alpha_i = [\sqrt{I}, \sqrt{I}\exp(\phi_i)]$, where I is the incident intensity of the balanced beams and $\phi_i = 0, \pi$. The total scattered intensity for each eigenvector is $2|s_i|^2 I$. Figure 2A shows a theoretical plot of S-matrix eigenvalue intensities, $|s|^2$, assuming $n = 3.6 + 0.0008i$ and slab thickness $a = 115.79$ μm (*12*). Multiple CPA resonances exist, occurring alternatively for even and odd eigenvectors.

If we work at a wavelength corresponding to a CPA resonance, such as the central minimum shown in Fig. 2A, then, upon varying the relative phase ϕ from 0 to π (keeping the two beam intensities constant and equal), the system goes from enhanced scattering (red curve) to nearly zero scattering (blue curve). Intermediate values of ϕ do not correspond to a single S-matrix eigenstate, so the scattered intensity interpolates between the extremal values. The black curve in Fig. 2A shows the expected scattered intensity for incident beams neglecting their interference, $2(R + T)I$. At the CPA resonance, it lies roughly a factor of 2 below the scattered intensity of the even (red) mode, demonstrating substantial coherent reduction of absorption for this mode. This is due to constructive interference in this mode for escape from the cavity, reducing its total absorption; other, more complicated structures allow even larger contrast between the CPA mode and the "scattered" mode (*11*). There also exist "phase-insensitive" points between each pair of CPA resonances, seen in Fig. 2A where the red and blue curves cross. Here, the scattered intensity is completely independent of the relative phase of the two input beams and equal to the value for incoherent illumination.

The experimental data (Fig. 2, E to G) are in good agreement with the theoretical predictions (Fig. 2, B to D). The theoretical plots show the normalized total output intensity at three representative values of the wavelength, indicated by the corresponding labels (b to d) in Fig. 2A. They show, respectively, an odd-parity CPA resonance (Fig. 2B); an intermediate wavelength, with a smaller total intensity variation with ϕ but still a factor of ~2.5 in the scattering of the even- and odd-parity beams (Fig. 2C); and a phase-insensitive point (Fig. 2D). Also shown, along with the total output intensity, are the intensities as measured on the left and right. Generally, these two intensities have maximum attenuation at different values of ϕ. However at the wavelength corresponding to the CPA resonance (Fig. 2B), their minima coincide at a single ϕ (0 or π), producing an absorption contrast of several orders of magnitude. At the phase-insensitive point (Fig. 2D), the left and right outputs are precisely out of phase; varying ϕ leaves the total output unchanged but switches the dominant output between left and right.

A convenient figure of merit for how close the experiment comes to the exact CPA condition is the "modulation depth" $M(\lambda) = \max(I_{out})/\min(I_{out})$, the ratio of the maximum to minimum total output intensity as we vary ϕ. The observed values as a function of λ are shown in Fig. 3A. For a device satisfying the exact CPA condition, $\min(I_{out}) \to 0$ and so $M \to \infty$. This does not occur in the present device because we slightly miss the CPA condition by tuning only one parameter, λ, leading to a maximum modulation depth of ~10^4 to 10^5.

However, the limiting factors in the experiment are the temporal and spatial coherence of the laser, reducing $M(\lambda)$ to ~10^2. The finite laser linewidth (0.18 nm) "smears out" the CPA resonances, which are optimized for a monochromatic input. This effect can be partially compensated by filtering the output through a spectrometer [resolution ≈ 0.05 nm (*12*)]. This finite resolution of the spectrometer can be incorporated into the analysis, and the resulting theoretical curve, shown in Fig. 3A, agrees well with the experimental data. The dual role of interference in both enhancing and suppressing absorption can be seen more clearly in Fig. 3B, which compares the maximum and minimum output intensities to $2(R + T)$, the expected output intensity for two incoherent input beams. At the CPA resonant wavelength, the minimum output intensity is less than 1% of the input, while the incoherent

illumination gives ~35% output. When the phase is adjusted to maximize the scattering, the output reaches ~70%.

Although we have demonstrated coherent reduction of absorption in our experiment, this effect should be distinguished from the phenomenon of electromagnetically induced transparency, in which absorption is suppressed by coherently driving the absorbing medium itself (*24*), instead of by enhancing escape from the cavity by constructive interference, as in our system.

Because this optical effect is easily realized in silicon, coherent perfect absorbers may enable novel functionalities in silicon integrated photonic circuits of the type envisioned for next-generation optical communications and computing applications (*25*) as well as for coherent laser spectroscopy. The simplest versions of the device immediately would serve as compact on-chip interferometers, which absorb or scatter the input beams instead of steering them. Although our current CPA operates near the silicon band edge, it should be possible to fabricate devices in which an additional parameter tunes the absorption coefficient independently of λ (e.g., by free carrier injection or by optical pumping), allowing one to fix the operating wavelength by design. Direct–band gap semiconductors also are suitable materials for CPAs, assuming that fluorescent emission can be tolerated or avoided in a specific application. Recent theoretical work has proposed a fascinating extension of the CPA concept, suitable for direct–band gap materials: Systems with balanced gain and loss can function simultaneously as a CPA and as a laser (i.e., as an interferometric amplifier-attenuator) (*26*, *27*). The CPA effect is not immediately applicable to photovoltaic or stealth technology because it is a narrow-band effect requiring coherent inputs.

More generally, the exact time-reversal symmetry property that relates laser emission to coherent perfect absorption implies that an arbitrarily complicated scattering system can be made to perfectly absorb at discrete frequencies if its imaginary refractive index can be tuned continuously over a reasonable range of values, and if appropriate coherent incident beams can be imposed. Progress in these areas would open up interesting new avenues for future research and applications.

References and Notes

1. E. L. Hahn, *Phys. Rev.* **80**, 580 (1950).
2. G. Bergmann, *Phys. Rep.* **107**, 1 (1984).
3. Y. Kuga, A. Ishimaru, *J. Opt. Soc. Am. A* **1**, 831 (1984).
4. M. P. Van Albada, A. Lagendijk, *Phys. Rev. Lett.* **55**, 2692 (1985).
5. P. E. Wolf, G. Maret, *Phys. Rev. Lett.* **55**, 2696 (1985).
6. C. H. Lewenkopf, H. A. Weidenmuller, *Ann. Phys.* **212**, 53 (1991).
7. M. Fink *et al.*, *Rep. Prog. Phys.* **63**, 1933 (2000).
8. J. de Rosny, M. Fink, *Phys. Rev. Lett.* **89**, 124301 (2002).
9. De Rosny and Fink (*8*) demonstrated a process of perfect absorption of time-reversed acoustic waves, but this requires a dynamic sink that is driven externally with appropriate amplitude and phase. This process is not related to time-reversed lasing.
10. G. Lerosey, J. de Rosny, A. Tourin, M. Fink, *Science* **315**, 1120 (2007).
11. Y. D. Chong, L. Ge, H. Cao, A. D. Stone, *Phys. Rev. Lett.* **105**, 053901 (2010).
12. See supporting material on *Science* Online.
13. A. E. Siegman, *Phys. Rev. A* **39**, 1253 (1989).
14. W. A. Hamel, J. P. Woerdman, *Phys. Rev. A* **40**, 2785 (1989).
15. R. H. Yan, R. J. Simes, L. A. Coldren, *IEEE Photon. Technol. Lett.* **1**, 273 (1989).
16. K.-K. Law, R. H. Yan, J. L. Merz, L. A. Coldren, *Appl. Phys. Lett.* **56**, 1886 (1990).
17. K.-K. Law, R. H. Yan, L. A. Coldren, J. L. Merz, *Appl. Phys. Lett.* **57**, 1345 (1990).
18. J. F. Heffernan, M. H. Moloney, J. Hegarty, J. S. Roberts, M. Whitehead, *Appl. Phys. Lett.* **58**, 2877 (1991).
19. K. Kishino *et al.*, *IEEE J. Quantum Electron.* **27**, 2025 (1991).
20. M. S. Ünlü, K. Kishino, H. J. Liaw, H. Morkoç, *J. Appl. Phys.* **71**, 4049 (1992).
21. M. Cai, O. Painter, K. J. Vahala, *Phys. Rev. Lett.* **85**, 74 (2000).
22. A. Yariv, *IEEE Photon. Technol. Lett.* **14**, 483 (2002).
23. J. R. Tischler, M. S. Bradley, V. Bulović, *Opt. Lett.* **31**, 2045 (2006).
24. S. E. Harris, *Phys. Today* **50**, 36 (1997).
25. M. Lipson, *J. Lightwave Technol.* **23**, 4222 (2005).
26. S. Longhi, *Phys. Rev. A* **82**, 031801(R) (2010).
27. Y. D. Chong, L. Ge, A. D. Stone, http://arxiv4.library.cornell.edu/abs/1008.5156v1 (2010).

28. Supported by NSF grants DMR-0808937 and DMR-0908437 and by seed funding from the Yale NSF-MRSEC (DMR-0520495). We thank E. Dufresne for use of his laser facility, and D. Miller and J. Bleuse for drawing our attention to the literature on asymmetric Fabry-Perot modulators and resonant cavity-enhanced photodetectors, respectively.

Supporting Online Material

www.sciencemag.org/cgi/content/full/331/6019/889/DC1
Materials and Methods
Figs. S1 and S2

22 November 2010; accepted 19 January 2011
10.1126/science.1200735

Quantum Reflection of He_2 Several Nanometers Above a Grating Surface

Bum Suk Zhao,* Gerard Meijer, Wieland Schöllkopf

Quantum reflection allows an atom or molecule to be reflected from a solid before it reaches the region where it would encounter the repulsive potential of the surface. We observed nondestructive scattering of the helium dimer (He_2), which has a binding energy of 10^{-7} electron volt, from a solid reflection grating. We scattered a beam containing the dimer as well as atomic helium and larger clusters, but could differentiate the dimer by its diffraction angle. Helium dimers are quantum reflected tens of nanometers above the surface, where the surface-induced forces are too weak to dissociate the fragile bond.

A neutral atom or molecule approaching a solid surface experiences an attractive force caused by the van der Waals atom-surface interaction potential, as sketched in Fig. 1A. In a classical picture, the particle accelerates toward the surface until it scatters back from the steep repulsive-potential branch. In quantum-mechanical scattering, a wave packet approaching the surface exhibits a nonvanishing reflection coefficient even when it is in the attractive part of the potential. Thus, despite the force acting toward the surface, there is some probability that the particle will reflect tens of nanometers or more above the surface, without ever colliding with the repulsive potential wall. The probability for this counterintuitive effect, termed quantum reflection, even approaches unity in the low-energy limit of the incident particle [e.g., (*1*)]. Quantum reflection from a solid was first observed by Shimizu for ultracold metastable Ne (*2*) and He (*3*) atoms. Later, it was also observed with helium atom beams (*4*, *5*). Here, we demonstrate that quantum reflection allows for nondestructive scattering of extremely fragile helium dimers from a ruled reflection grating.

The van der Waals–bound dimer of two ground-state helium atoms, He_2, is the most fragile ground-state molecule known (*6*, *7*). The binding energy of 10^{-7} eV leads to an exceptionally large bond length (mean internuclear distance) of 5.2 nm (*8*). The helium dimer is a quantum system because the probability for He_2 to be found in a classically forbidden state, where the internuclear separation is larger than the system's classical outer turning point, is more than 80% (Fig. 1B). Moreover, because rotational or vibrational excitation leads to dissociation, there are no excited bound states. These distinctive features have made He_2 an attractive model system for computational methods in quantum chemistry.

Trying to observe nondestructive scattering of He_2 from a solid surface appears to be an ill-conceived experiment. Even at grazing incidence, where the kinetic energy associated with the dimer's momentum component perpendicular to the surface can be smaller than the binding energy, the dimer is likely to be torn apart by the forces exerted on both atoms in the surface–potential-well region sketched in Fig. 1A. The potential-well depth is typically ~5 meV, hence,

Fritz-Haber-Institut der Max-Planck-Gesellschaft, Faradayweg 4-6, 14195 Berlin, Germany.

*To whom correspondence should be addressed. E-mail: zhao@fhi-berlin.mpg.de